

Strain and temperature dependence of the insulating phases of VO₂ near the metal-insulator transition

Joanna M. Atkin, Samuel Berweger, Emily K. Chavez, and Markus B. Raschke

Department of Physics, Department of Chemistry, and JILA, University of Colorado, Boulder, Colorado 80309, USA

Jinbo Cao, Wen Fan, and Junqiao Wu

Department of Materials Science and Engineering, University of California, Berkeley, California 94720, USA

(Received 21 July 2011; revised manuscript received 30 November 2011; published 5 January 2012)

In addition to its metal-insulator transition (MIT), VO₂ exhibits a rich phase behavior of insulating monoclinic (M1, M2) and triclinic (T) phases. By using micro-Raman spectroscopy and independent control of temperature and uniaxial strain in individual single-crystal microbeams, we map these insulating phases with their associated structural changes as represented by their respective phonon frequencies. The competition between these structural forms is dictated by the internal strain due to differing lattice constants, the experimentally applied external strain, and the temperature-dependent phase stability. We identify the nature of the triclinic phase as a continuously distorted variant of the M1 monoclinic phase, while a discontinuous transition into the M2 phase occurs from both the M1 and T phases. The results suggest that understanding the driving forces that determine the interplay between M1, M2, and T phases near the MIT could be critical for the identification of the underlying mechanism behind the MIT itself.

DOI: [10.1103/PhysRevB.85.020101](https://doi.org/10.1103/PhysRevB.85.020101)

PACS number(s): 74.25.nd, 61.50.Ks, 74.62.—c

Vanadium dioxide has been one of the most widely studied transition-metal oxides that exhibit a metal-insulator transition (MIT) due to its experimentally easily accessible transition temperature of ~ 341 K.^{1,2} The mechanism of the MIT is still widely debated, with the complexity of the problem related to the associated structural lattice changes^{3,4} and both Peierls and Mott signatures appearing during the transition.^{5–8} Interestingly, VO₂ is distinct from many other MIT materials due to the presence of several competing insulating phases, with their phase boundaries in a narrow temperature and strain range close to the MIT.⁹ These insulating phases have similar free energies and can readily be controlled by doping or strain.^{10–12} However, the insulating phases and their phase competition have received little attention despite evidence that they lead to different structural pathways for the MIT.^{13–15} Previously, the various phases have been difficult to access experimentally in a systematic way, in part due to a lack of reproducibility in crystal growth,¹⁶ phase reversibility, and strain control. Strain and changes in lattice constants between the phases also lead to domain formation, phase separation, and coupling in polycrystalline thin films,¹⁷ and cracking or degradation in bulk crystals on cycling through the MIT.¹⁸ In addition, the insulating phases can be difficult to distinguish in electrical transport and x-ray diffraction (XRD) measurements.^{19,20}

Here, we independently control uniaxial strain and temperature in order to investigate their influence on the crystallographic phases in freestanding VO₂ microcrystals. These microcrystals, typically in the form of beams²¹ with a small rectangular cross section, can withstand high elastic strain without deformation or degradation.²² By using phonon-Raman spectroscopy to identify the crystal lattice structure, we resolve the monoclinic M1, monoclinic M2, and triclinic T insulating phases and their transitions induced by temperature or strain. The triclinic phase is found to emerge as an intermediate structure close to room temperature

from a continuous distortion of the M1 lattice. The M2 phase, by contrast, shows a discontinuous transition in lattice organization when emerging from either the M1 or the T phase.

For the experiments, single-crystal VO₂ microbeams are grown on an oxidized silicon substrate by vapor phase transport, as described previously.²¹ Suitable crystals with lengths greater than 60 μm and widths larger than 2 μm are transferred onto a flexible polycarbonate substrate (thickness 0.8 mm, width 5 mm, length 20 mm) and glued at both of their ends with silver epoxy [Fig. 1(a)]. A resistive heater and thermocouple are also attached to the substrate for temperature control within ± 0.5 K. These devices are then mounted into a micrometer-controlled stage to exert tensile or compressive uniaxial strain on the beams along the c_R crystallographic direction by buckling the substrate [Fig. 1(a)]. With a typical beam width > 2 μm and beam thickness $\lesssim 1$ μm , substantially less than the thickness of the substrate, we ensure effectively uniform stress across the cross section of the rod.

Raman spectra are measured using a home-built micro-Raman system in epi-illumination and detection geometry. HeNe laser light ($\lambda = 632.8$ nm) is focused with an objective [Olympus LMPlanFl N, 0.8 numerical aperture], with a total power at the sample $\lesssim 0.01$ mW to minimize heating effects (fluence < 1.3 kW/cm²). The Raman scattered light is spectrally filtered with a 160 cm⁻¹ cutoff filter and detected with a spectrometer and N₂(l)-cooled CCD with 1 cm⁻¹ resolution (Princeton Instruments and Acton Research). The incident light is polarized along the microbeam (c_R) in order to maximize the signal, with unpolarized detection, yielding a superposition of the A_g and B_g modes.²³ Figure 1(b) shows representative spectra for the monoclinic M1, monoclinic M2, and triclinic T insulating phases. Our measured M1 spectrum is consistent with previous measurements on bulk and microcrystalline VO₂,¹³ with the Raman-active modes predicted by its space group C_{2h}^5 .^{23,24} The M2 Raman response [space group C_{2h}^3 (Ref. 25)] is distinguished from the M1 primarily

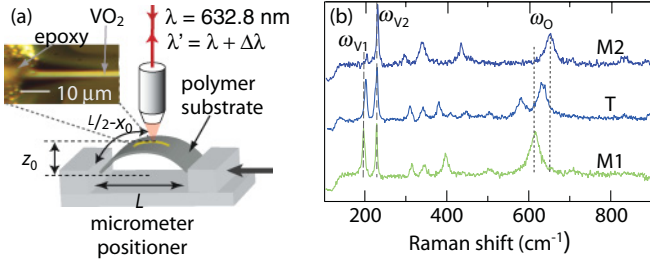


FIG. 1. (Color online) (a) Schematic of the experimental configuration, with a photograph of a representative VO₂ microbeam sample. The substrate is buckled up or down with a micrometer stage to control the degree of tensile or compressive strain, respectively. (b) Characteristic Raman spectra for the M1, triclinic (T), and M2 insulating phases.

by the blueshift of the dominant 610 cm⁻¹ phonon frequency (denoted ω_O) and the associated intensity decrease and a slight spectral shift of the 189 cm⁻¹ mode (ω_{V1}). To the best of our knowledge, the triclinic phase has not been extensively studied in the literature, but has been identified in Raman spectroscopic measurements through the splitting of the ω_O phonon.¹¹ Using isotope substitution and density functional theory calculations, it has been established that the two low-frequency phonons (ω_{V1} and ω_{V2}) correspond to V-V lattice motion, and all other distinguishable peaks relate to V-O bonding.¹¹

Figure 2(a) shows the evolution in Raman spectra with increasing tensile strain at room temperature. The strain ϵ (%) imposed on the VO₂ beam can be estimated from

$$\epsilon = 3z_0 \frac{d}{2} \left(\frac{2}{L} \right)^3 \left(\frac{L}{2} - x_0 \right), \quad (1)$$

with the horizontal distance between the two lever points L , the thickness of the polymer substrate d , the position of the microbeam with respect to the center of the substrate x_0 , and its vertical displacement at its center z_0 [Fig. 1(a)].

For beams under compressive strain or weak tensile strain (<1%), the Raman spectra display the characteristic M1 modes. As the tensile strain increases, a small redshift of ω_O occurs, accompanied by the emergence of an additional peak of lower frequency. The two peaks continue to split and shift until, at a critical strain value, there is an abrupt transition into the M2 phase, and the lower-frequency ω_O peak disappears.

The frequency shifts of the Raman modes with increasing strain, as extracted from Lorentzian line fits, are shown in Fig. 2(b). In addition to the pronounced change in the ω_O peak position, the lower-frequency Raman modes, with the exception of the ~ 340 cm⁻¹ mode, also experience frequency shifts, with the 310 and 394 cm⁻¹ V-O phonons softening and the low-frequency V-V phonons hardening. This phonon behavior is characteristic of the structural properties of the triclinic phase, and is distinct from simple strain effects on the monoclinic lattice.^{11,26} Figures 2(d) and 2(e) show magnified views of ω_O and ω_{V1} and ω_{V2} phonon behavior, with the colorbar representing the phase based on the spectral position of the peaks and the continuous M1-T phase transition.

The observed phase behavior was reproducible across several microbeam samples with varying lengths and widths. However, the applied strain at which the T and M2 phases appeared varied by $\pm 1\%$, due to a range of external strain offsets that arise from the gluing procedure of the VO₂ beams onto the substrate. To account for this variable offset, we have renormalized the strain variations against previous results for relative consistency.²⁷ We also note that the glue is of limited rigidity, particularly at high temperatures, leading to strain relaxation over repeated measurements and limiting reproducibility [e.g., Fig. 2(c), demonstrating the instability at the T-M2 transition].

Based on the spectral position of ω_O as a fingerprint for the three different phases, we map their strain-temperature phase diagram as shown in Fig. 3(a). For temperatures below ~ 305 K, we observe a M1-T-M2 structural transition with increasing tensile strain, with the T phase appearing for a wide

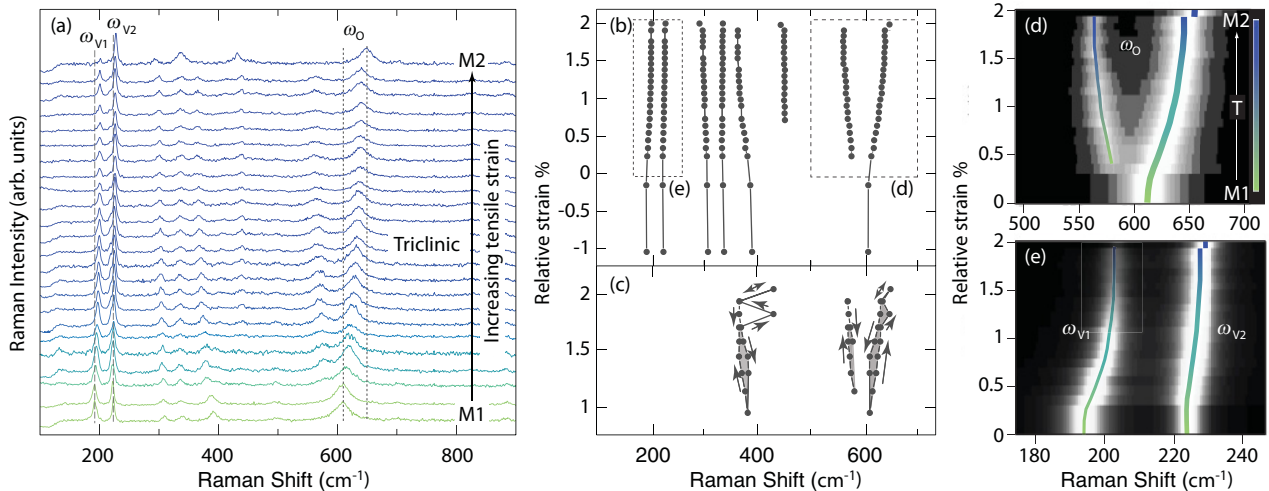


FIG. 2. (Color online) (a) Raman spectra of VO₂ showing the evolution in phonon modes as the VO₂ microcrystal is subjected to increasing tensile strain at room temperature. (b) Peak positions determined from Lorentzian fitting for the data shown in (a). (d) and (e) Closeup view of ω_O and ω_{V1} and ω_{V2} phonon frequency evolution. (c) Hysteresis in strain behavior demonstrating relaxation under high strain conditions.

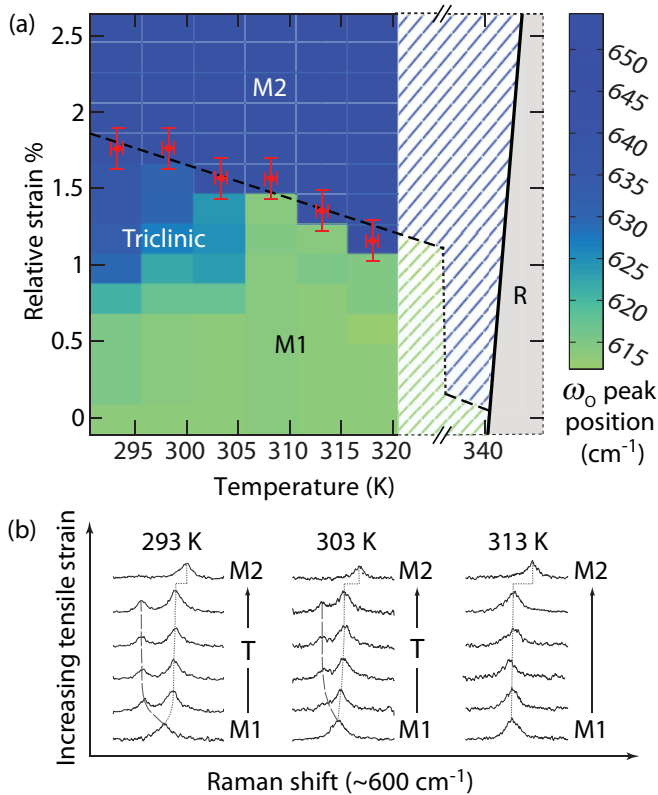


FIG. 3. (Color online) (a) Strain-temperature phase diagram of the insulating phases of VO_2 represented via the ω_0 phonon frequency shift. The error bars are estimated from the relaxation effect noted in Fig. 2(c). The shaded region and solid black line show qualitative measurements of the MIT, where a precise peak position analysis was not possible. (b) Representative change in ω_0 position with strain at different temperatures, showing the direct M1-M2 transition at high temperatures.

range of strain values. Above ~ 305 K, the T phase vanishes and an abrupt M1-M2 transition occurs [Fig. 3(b)]. Because of the strain relaxation mentioned above at high temperatures, we are not able to extend the measurements up to the MIT. Qualitatively the metallic phase was determined through the change in reflectivity of the VO_2 beam as shown by the solid black phase boundary. We confirm the expected increase in MIT temperature at high tensile strain. Under compressive strain, we found that the microbeams remain in the M1 phase up to the MIT, which occurs at lower temperatures for higher compressive strain (not shown). As expected, because of the weak substrate interactions and uniaxial strain, no domain formation is observed.¹³ Instead, the metallic phase nucleates at one end of the beam and only one phase boundary is seen moving across the beam through the phase transition.

The existence of several insulating phases was first observed in doped VO_2 bulk material soon after the discovery of the MIT. Subsequently the two monoclinic structures M1 and M2, and triclinic T phase^{10,28} (sometimes termed M3 in the literature^{11,29}) were identified. In the M1 phase, the vanadium atoms are paired and tilted, forming zigzag chains along the c_R axis. In contrast, the M2 phase has two distinct

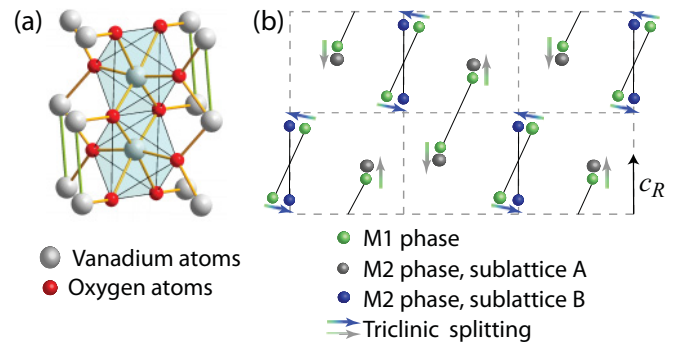


FIG. 4. (Color online) (a) VO_2 crystal structure, showing the oxygen octahedra (red) arranged around the paired and tilted vanadium sublattices (gray). (b) Positions of the vanadium atoms in the M1 (green) and M2 (dark gray, blue) phases. The triclinic phase is intermediate between these two states.

sublattices of V atoms: In sublattice A the vanadium atoms are paired along the c_R axis but not tilted, and in sublattice B they are tilted perpendicular to the c_R axis but unpaired^{29,30} [see Figs. 4(a) and 4(b)]. Through a combination of nuclear magnetic resonance, electron paramagnetic resonance, and XRD measurements,^{10,11} the triclinic phase was found to be an intermediate phase where a progressive distinction between the two vanadium sublattices occurs, with depairing in one of the vanadium chains accompanying untilting in the other.

Previous estimates on the extent of the T phase, based on extrapolations of limited data close to the M1-T and T-M2 phase boundaries, disagreed as to whether a T-R transition is possible.²⁹ Our direct measurement of the extent of the T phase and observations of a M1-M2 transition clarifies that there is no T-R boundary. Our M1-M2 phase boundary is in good agreement with previous measurements using scanning electron microscopy (SEM) characterization.²⁷ The phase boundary we determine for the onset of the M2 phase from either T or M1 has a slope comparable to these SEM results.

The abrupt M1-M2 and T-M2 transitions may be an unexpected observation as the M1 and T phases can be viewed as superpositions of two M2-type lattice distortions.^{26,31} Initially, the dimerization in only one sublattice of the M2 phase led to the suggestion of an electron-correlation contribution to the band-gap opening via a Mott-Hubbard process.¹² Furthermore, since the T phase can substantially reduce the M1-M2 discontinuity and produce an almost-continuous transition between the M1 and M2 phases, it was concluded that the M1 and T phases were also of Mott-Hubbard character,³¹ in spite of the nonmagnetic properties of the M1 phase. More recent work, however, suggests that a band-theoretical approach can describe the insulating properties of both the M1 and M2 phases, provided that the antiferromagnetic nature of the M2 phase is considered.³² Conversely, it has been noted that the decrease in the MIT temperature with compressive strain is inconsistent with a band-theory description, since compression along the rutile c_R axis increases the splitting between the bonding and antibonding states and therefore should drive the system further into the insulating phase.³³

Our results demonstrate that different structural pathways into the metallic R phase are possible, with M1-R, M1-T-M2-R, and M1-M2-R transitions occurring for various combinations of strain and temperature. This confirms previous observations of a M2-R transition under high tensile strain.^{13,27} These results raise interesting questions about whether the mechanism for the MIT is universal or is different depending on whether the insulating phase is M1 or M2. The observation of a threshold resistivity for triggering the MIT in microbeams,^{34,35} regardless of strain and temperature conditions, hints that the M2 phase could be a universal transitional phase. Measurements on overhanging beams with no direct substrate interactions have occasionally but inconsistently indicated a brief, transient M2 phase immediately before the metallic transition, and we cannot exclude the possibility that a narrow region of the M2 phase exists along the rutile boundary regardless of strain.

In summary, we have observed that the triclinic and M2 phases occur over a wide range of strain in individual, homogeneous VO₂ microbeams subjected to external uniaxial strain. The presence of these phases is significant as it indicates

that the common assumption of a direct transition from M1-R will not always apply, and a complex interplay of insulating phases may occur depending on the interaction between VO₂ and the substrate, including clamping, lattice mismatch, and anisotropic strain, as well as lateral crystallite interactions in thin films. Single-crystalline microcrystals are ideal for studying the influence of strain because of the lack of extrinsic crystallite interactions. Further study of well-controlled samples is necessary in order to determine the structurally driven versus electronic-driven contributions to the MIT, in the absence of complicating insulating phases. In particular, ultrafast time-resolved dynamics investigations with the samples initially in one of the different insulating structures may determine the intrinsic electronic contributions and clarify the importance of the M2 phase to the MIT.

The authors acknowledge support from the National Science Foundation (Grant No. DMR-1055938), Department of Energy Division of Materials Sciences and Engineering (Grant No. DE-SC0002197), and valuable discussions with Andrew Jones, Volker Eyert, and David Cobden.

-
- ¹F. J. Morin, *Phys. Rev. Lett.* **3**, 34 (1959).
²M. Imada, A. Fujimori, and Y. Tokura, *Rev. Mod. Phys.* **70**, 1039 (1998).
³G. Andersson, *Acta Chem. Scand.* **10**, 623 (1956).
⁴J. B. Goodenough, *Phys. Rev.* **117**, 1442 (1960).
⁵N. F. Mott, *Rev. Mod. Phys.* **40**, 677 (1968).
⁶A. Zylbersztein and N. F. Mott, *Phys. Rev. B* **11**, 4383 (1975).
⁷M. M. Qazilbash *et al.*, *Science* **318**, 1750 (2007).
⁸C. Kubler, H. Ehrke, R. Huber, R. Lopez, A. Halabica, R. F. Haglund, and A. Leitenstorfer, *Phys. Rev. Lett.* **99**, 116401 (2007).
⁹D. Paquet and P. Leroux-Hugon, *Phys. Rev. B* **22**, 5284 (1980).
¹⁰J. P. Pouget, H. Launois, T. Rice, P. D. Dernier, A. Gossard, G. Villeneuve, and P. Hagenmuller, *Phys. Rev. B* **10**, 1801 (1974).
¹¹C. Marini *et al.*, *Phys. Rev. B* **77**, 235111 (2008).
¹²J. P. Pouget, H. Launois, J. D'Haenens, P. Merenda, and T. Rice, *Phys. Rev. Lett.* **35**, 873 (1975).
¹³A. C. Jones, S. Berweger, J. Wei, D. Cobden, and M. B. Raschke, *Nano Lett.* **10**, 1574 (2010).
¹⁴J. I. Sohn, H. J. Joo, D. Ahn, H. H. Lee, A. E. Porter, K. Kim, D. J. Kang, and M. E. Welland, *Nano Lett.* **9**, 3392 (2009).
¹⁵T. Yao *et al.*, *Phys. Rev. Lett.* **105**, 226405 (2010).
¹⁶J. M. Booth and P. S. Casey, *ACS Appl. Mater. Interfaces* **1**, 1899 (2009).
¹⁷A. Frenzel, M. M. Qazilbash, M. Brehm, B. G. Chae, B. J. Kim, H. T. Kim, A. V. Balatsky, F. Keilmann, and D. N. Basov, *Phys. Rev. B* **80**, 115115 (2009).
¹⁸D. Maurer and A. Leue, *Mater. Sci. Eng. A* **370**, 440 (2004).
¹⁹B. Chamberland, *J. Solid State Chem.* **7**, 377 (1973).
²⁰J. W. Pierce and J. B. Goodenough, *Phys. Rev. B* **5**, 4104 (1972).
²¹B. S. Guiton, Q. Gu, A. L. Prieto, M. S. Gudiksen, and H. Park, *J. Am. Chem. Soc.* **127**, 498 (2005).
²²J. Cao *et al.*, *Nat. Nanotechnol.* **4**, 732 (2009).
²³P. Schilbe, *Physica B* **316**, 600 (2002).
²⁴E. U. Donev, R. Lopez, L. C. Feldman, and R. F. Haglund, *Nano Lett.* **9**, 702 (2009).
²⁵V. Eyert, *Ann. Phys.* **11**, 650 (2002).
²⁶A. Tselev, I. A. Luk'yanchuk, I. N. Ivanov, J. D. Budai, J. Z. Tischler, E. Strelcov, A. Kolmakov, and S. V. Kalinin, *Nano Lett.* **10**, 4409 (2010).
²⁷J. Cao *et al.*, *Nano Lett.* **10**, 2667 (2010).
²⁸G. Villeneuve, M. Drillon, and P. Hagenmuller, *Mater. Res. Bull.* **8**, 1111 (1973).
²⁹M. Marezio, D. B. McWhan, J. P. Remeika, and P. D. Dernier, *Phys. Rev. B* **5**, 2541 (1972).
³⁰J. Galy and G. Miehe, *Solid State Sci.* **1**, 433 (1999).
³¹T. M. Rice, H. Launois, and J. P. Pouget, *Phys. Rev. Lett.* **73**, 3042 (1994).
³²V. Eyert, *Phys. Rev. Lett.* **107**, 016401 (2011).
³³B. Lazarovits, K. Kim, K. Haule, and G. Kotliar, *Phys. Rev. B* **81**, 115117 (2010).
³⁴J. Cao, W. Fan, K. Chen, N. Tamura, M. Kunz, V. Eyert, and J. Wu, *Phys. Rev. B* **82**, 241101 (2010).
³⁵J. Wei, Z. Wang, W. Chen, and D. H. Cobden, *Nat. Nanotechnol.* **4**, 420 (2009).